

Metallic transport of hard core bosons

Sauri Bhattacharyya¹, Ayush De², Snir Gazit^{2,3} and Assa Auerbach¹

¹*Physics Department, Technion, 32000 Haifa, Israel*

²*The Racah Institute of Physics, The Hebrew University of Jerusalem, Jerusalem 9190401, Israel*

³*The Fritz Haber Research Center for Molecular Dynamics, The Hebrew University of Jerusalem, Jerusalem 91904, Israel*

(Dated: November 29, 2023)

Conductivities and Hall coefficients of two dimensional hard core bosons are calculated using the thermodynamic expansions of Kubo formulas. At temperatures above the superfluid transition, the resistivity rises linearly and is weakly dependent on boson filling. The zeroth order Hall coefficient diverges toward zero and unit fillings, and reverses its sign at half filling. The correction terms, which are calculated up to fourth (Krylov) orders, do not alter this behavior. The high temperature thermal Hall coefficient is reversed relative to the electric Hall coefficient. We discuss relevance of HCB transport to the metallic state of short coherence length superconductors.

I. INTRODUCTION

Two dimensional Hard Core Bosons (HCB) is a paradigmatic model of strongly interacting lattice bosons, and short coherence length superconductors. HCB have modeled ⁴He superfluid films [1], cold optical-lattice bosons between Mott insulator phases [2, 3], low capacitance Josephson junction arrays [4, 5], and the superconducting fluctuations of cuprates [6, 7].

HCB density-temperature (n - T) phase diagram has been well explored by numerical simulations of the spin half quantum XY model, using sign-free Quantum Monte Carlo (QMC) averaging [8–10]. Below the Berezinskii [11], Kosterlitz and Thouless [12] (BKT) temperature $T_{\text{BKT}}(n)$, which is maximized at $n = \frac{1}{2}$, HCB exhibit zero resistance and a finite superfluid stiffness, which can be explained by the *classical XY* model. In a narrow regime of short range phase correlations above $T_{\text{BKT}}(n)$, Halperin and Nelson (HN) [13] showed that the resistivity rises due to proliferation of free vortices. In order to apply HN theory for the HCB resistivity, we need to know the “normal metal” resistivity, which is defined at a temperature where the free vortices separation is reduced to the lattice constant scale.

However, the “normal metal” phase of HCB phase has received much less attention. This may be attributed to the inability of Boltzmann’s equation to properly account for hard core interactions and lattice Umklapp scattering, especially near half filling where the mean free path would be estimated as less than a lattice constant.

The alternative is to directly compute real-frequency Kubo formulas, which faces severe numerical challenges. Exact diagonalizations for the eigenstates (Lehmann) representation are exponentially costly in lattice size. Analytic continuation of QMC data to real frequencies is ill-posed at frequencies lower than the temperature [14], which requires the use of proxies for the DC limit [15].

On the other hand, thermodynamic approaches to Kubo formulas [16, 17] enjoy the advantage of calculating equilibrium expectation values and static susceptibili-

ties. These are amenable to well established statistical-mechanics tools. For example, high temperature expansion, variational wavefunctions, and imaginary-time QMC avoid the high memory cost of exact diagonalizations, and the numerical pitfalls of analytic continuation.

In this paper we apply two thermodynamic approaches to the HCB model. (i) A continued fraction (CF) expansion [18] combined with a variational extrapolation of recurrences [19, 20]. (ii) New thermodynamic summation formulas of Hall and thermal Hall coefficients [21, 22]. These formulas were previously applied to narrow gap semimetals [23], and to the Hubbard [24] and tJ models [25] of strongly interacting electrons.

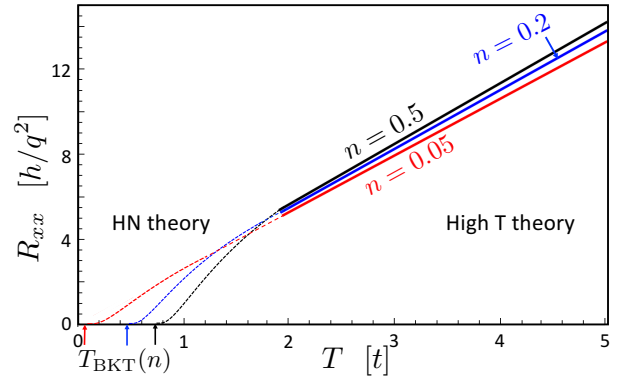


FIG. 1. Resistivity versus temperature of HCB for several densities $0 < n < \frac{1}{2}$. (R_{xx} is symmetric for $n \rightarrow 1 - n$). At high temperatures (solid lines) R_{xx} is calculated by Gaussian extrapolation of 5 lowest order recurrences, see Fig. 4. The resistivities vanish exponentially (dashed lines) toward the superconducting transition at $T_{\text{BKT}} \simeq 2.8tn(1 - n)$, following Halperin and Nelson’s (HN) theory, Eq. 26.

Our main results are as follows. As shown in Fig. 1, HCB resistivity rises with a linear slope whose value is insensitive to the density even down to 5% filling. This density independence is linked to a cancellation between the kinetic energy and the current relaxation time.

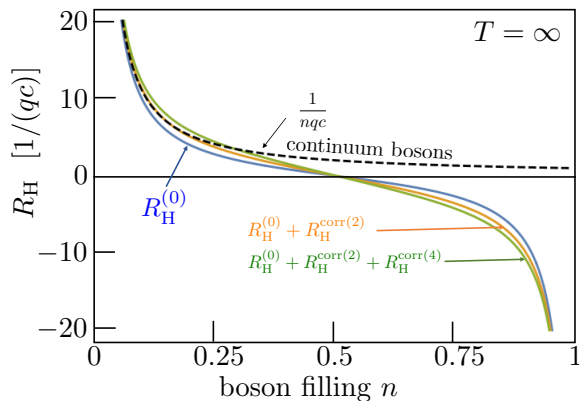


FIG. 2. Density dependent Hall coefficient $R_H(n)$ of HCB on a square lattice at high temperature. $R_H^{(0)}$, R_H^{corr} are defined in Eqs. (19) and (22). Convergence up to fourth order corrections is shown by the yellow and green curves. The Hall sign change at half filling is a consequence of the the hard core interactions on the lattice.

In Fig. 2 we plot the density dependent Hall coefficient, whose sign is reversed at half filling relative to the Galilean result of continuum bosons. The correction terms of the thermodynamic formula are calculated up to fourth order and shown to be relatively unimportant. We also obtain the thermal Hall coefficient, which is opposite in sign to the Hall effect, reflecting a “cooling” effect of the Hall current near half filling.

This paper is organized as follows. In Section II the HCB model is defined. Section III reviews the continued fraction expansion of the conductivity and the gaussian extrapolation of its recurrents. Section IV describes the zeroth Hall coefficient term evaluated by a high temperature expansion and extended to low temperatures by QMC. Section IV A describes the calculation of the correction term up to fourth order. This calculation is crucially important for estimating the accuracy of the zeroth term. Section VI calculates the thermal Hall coefficient. We conclude by a summary and discussion of relevancy of our results to experiments, with particular emphasis on normal phase transport of short coherence-length superconductors such as cuprates. Experiments in cold atoms trapped in an optical lattice are also proposed.

II. HARD CORE BOSONS MODEL

The HCB creation and density operators at site i are \tilde{a}_i^\dagger, n_i respectively, which obey $[n_i, \tilde{a}_j^\dagger] = \delta_{ij} \tilde{a}_i^\dagger$. The HCB constraint $(\tilde{a}_i^\dagger)^2 = 0$ is faithfully represented by spin half operators, $\tilde{a}_i^\dagger \rightarrow S_i^+, n_i - \frac{1}{2} \rightarrow S_i^z$ (setting $\hbar \rightarrow 1$). On a square lattice with unit lattice constant, and total area

A , we consider the gauged Hamiltonian of HCB,

$$H = -t \left(\sum_{\langle ij \rangle} e^{-i\frac{q}{c} A_{ij}} S_i^+ S_j^- + h.c \right) - \mu \sum_i S_i^z, \quad (1)$$

where μ is the chemical potential and q/c is the boson charge over velocity of light. $\mathbf{A}_{ij} = -\frac{\mathbf{r}_i + \mathbf{r}_j}{4} \times \mathbf{B} \cdot \mathbf{r}_{ij}$ introduces a uniform magnetic field $\mathbf{B} \parallel \mathbf{z}$. The HCB charge polarizations, currents and magnetization operators are respectively represented by,

$$\begin{aligned} \mathbf{P} &= q \sum_i \mathbf{r}_i S_i^z, \quad \mathbf{j} = i[H, \mathbf{P}] = \sum_{\langle ij \rangle} \mathbf{j}_{ij}, \\ j_{ij}^\alpha &= -iqt(S_i^+ S_j^- - S_i^- S_j^+)(r_j^\alpha - r_i^\alpha), \\ M &= \frac{1}{4c} \sum_{\langle ij \rangle} (\mathbf{r}_i + \mathbf{r}_j) \times \mathbf{j}_{ij}. \end{aligned} \quad (2)$$

Here \mathbf{r}_i denotes the position of site i . The density dependent $T_{\text{BKT}}(n)$ for HCB on the square lattice [9, 26, 27] is

$$T_{\text{BKT}}(n) \simeq 2.8tn(1-n). \quad (3)$$

III. DC RESISTIVITY

The DC longitudinal conductivity is given by the CF expansion,

$$\sigma_{xx}^{\text{dc}} = \chi_{\text{csr}} \lim_{\varepsilon \rightarrow 0^+} \text{Im} \frac{1}{-i\varepsilon + \frac{\Delta_1^2}{-i\varepsilon + \frac{\Delta_2^2}{\ddots}}} \quad (4)$$

where χ_{csr} is the conductivity sum rule (CSR),

$$\chi_{\text{csr}} = \frac{1}{A} \text{Im} \langle [P^x, j^x] \rangle \quad (5)$$

and $\Delta_k, k = 1, \dots, k_{\text{max}}$ are the calculated recurrents. The recurrents are obtained from the conductivity moments, which are calculated as thermodynamic expectation values,

$$\mu_{2k} = -\frac{1}{A} \text{Re} \langle [j^x, \overbrace{[H, [H, \dots [H, j^x]]}]^{2k-1}} \dots] \rangle, \quad (6)$$

j^x is the uniform current in the x direction defined in Eq. (2).

The CSR and the μ_{2k} are expanded in powers of inverse temperature β as described in Appendix B. The CSR up to order β^3 is given by,

$$\begin{aligned} \chi_{\text{csr}} &= \beta q^2 t^2 n (1-n) \left(2 \right. \\ &\quad \left. + \frac{(\beta t)^2}{3} (1-n)^2 (-3 + 10n(1-n)) \right). \end{aligned} \quad (7)$$

$2k$	$\bar{\mu}_{2k}/(\beta t^{2k})$
2	$16n(1-n)$
4	$64n(1-n)n(3+4n-4n^2)$
6	$32n(1-n)(177+356n-356n^2)$
8	$128n(1-n)(1979+7520n-10432n^2+7040n^3-6560n^4+3648n^5-1216n^6)$
10	$128n(1-n)(119200+856443n-1386927n^2+1358488n^3-1459972n^4+1040272n^5-519088n^6+147712n^7-36928n^8)$

TABLE I. Normalized conductivity moments $\bar{\mu}_{2k} = \mu_{2k}/\chi_{\text{csr}}$ as functions of density n at leading order in β .

The five lowest normalized moments $\bar{\mu}_{2k} = \mu_{2k}/\chi_{\text{csr}}$ are shown in Table I. They involve traces over many operators which are evaluated by symbolic multiplication, as explained in Appendix D. The recurrences Δ_k in Eq. (4) are obtained from the normalized moments by the algebraic relations given in Appendix A. The five lowest order recurrences are,

$$\begin{aligned}
\Delta_1^2 &= \bar{\mu}_2, \\
\Delta_2^2 &= \frac{\bar{\mu}_4}{\bar{\mu}_2} - \bar{\mu}_2, \\
\Delta_3^2 &= \frac{\bar{\mu}_4^2 - \bar{\mu}_2\bar{\mu}_6}{\bar{\mu}_2^3 - \bar{\mu}_2\bar{\mu}_4}, \\
\Delta_4^2 &= \bar{\mu}_2 \frac{(\bar{\mu}_4^3 + \bar{\mu}_6^2 + \bar{\mu}_2^2\bar{\mu}_8 - \bar{\mu}_4(2\bar{\mu}_2\bar{\mu}_6 + \bar{\mu}_8))}{(\bar{\mu}_2^2 - \bar{\mu}_4)(\bar{\mu}_2\bar{\mu}_6 - \bar{\mu}_4^2)}, \\
\Delta_5^2 &= \frac{\bar{\mu}_4 - \bar{\mu}_2^2}{\bar{\mu}_4^2 - \bar{\mu}_2\bar{\mu}_6} \\
&\quad \times \frac{\bar{\mu}_{10}(\bar{\mu}_2\bar{\mu}_6 - \bar{\mu}_4^2) - \bar{\mu}_6^3 + 2\bar{\mu}_4\bar{\mu}_6\bar{\mu}_8 - \bar{\mu}_2\bar{\mu}_8^2}{\bar{\mu}_4^3 + \bar{\mu}_6^2 + \bar{\mu}_2^2\bar{\mu}_8 - \bar{\mu}_4(2\bar{\mu}_2\bar{\mu}_6 + \bar{\mu}_8)}. \quad (8)
\end{aligned}$$

In Fig. 3, the recurrences of Eqs. 8 are plotted for densities $0 < n < 1$.

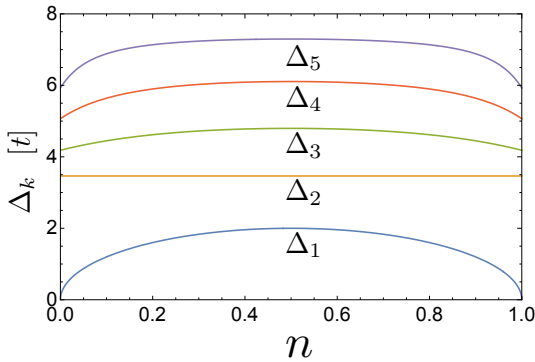


FIG. 3. Density dependence of the five lowest recurrences. The behavior of Δ_1 in Eq. (9) is largely responsible for the weak density dependence of the resistivity slopes in Fig. 1.

For the square lattice, the leading high temperature terms are $\chi_{\text{csr}} \propto \beta$, and $\Delta_k = \mathcal{O}(\beta^0)$. Thus conductivity goes as β , and the resistivity is asymptotically linear.

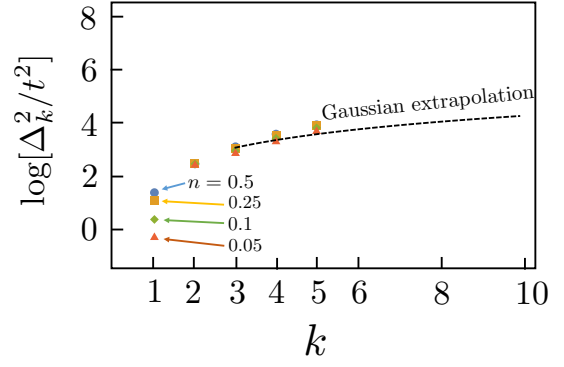


FIG. 4. High temperature conductivity recurrences of HCB. Solid circles are calculated recurrences, dashed line describes the Gaussian extrapolation based on the third to the fifth calculated recurrences at density $n = 0.3$.

In Fig. (4) the five lowest recurrences are depicted on a log-linear plot, for densities varying from 5%-50%. We note that the first recurrence is,

$$\Delta_1^2 = 16n(1-n)t^2. \quad (9)$$

We also notice in Figs. 3 and 4 that $\Delta_{k>1}$ exhibit a weaker density dependence.

A. Gaussian termination function

Having calculated the recurrences $\Delta_1, \Delta_2 \dots \Delta_{k_{\text{max}}}$, the CF in Eq. 4 depends on the imaginary part of an unknown termination function $G''_{k_{\text{max}}+1} = \lim_{\varepsilon \rightarrow 0} \text{Im}G_{k_{\text{max}}+1}(i\varepsilon)$,

$$\sigma_{xx}^{\text{dc}} = \chi_{\text{csr}} \frac{1}{\frac{\Delta_1^2}{\Delta_{k_{\text{max}}}^2 G''_{k_{\text{max}}+1}(0^+)}} \quad (10)$$

The variational extrapolation of recurrences (VER) method determines $G_{k_{\text{max}}+1}$ as follows.

For the HCB model at $n = 0.5$, VER yielded good agreement [19] between the extrapolated high temperature conductivity and the Kubo formula computed by exact diagonalization. The choice of a gaussian variational function,

$$F(\omega) = \frac{\sqrt{\pi}}{\Omega} \exp\left(-\frac{\omega^2}{\Omega^2}\right), \quad (11)$$

proved adequate. Its variational recurrences are,

$$\bar{\Delta}_k^2 = k \frac{\Omega^2}{2}. \quad (12)$$

In Fig. 4 we show a good fit of the dashed line to the computed recurrences $\Delta_3, \Delta_4, \Delta_5$, for the variational choice

$$\Omega^2 = \frac{2}{3} \Delta_3^2. \quad (13)$$

The corresponding termination function \bar{G}_6'' is determined by,

$$\text{Im}\bar{F}(\omega \rightarrow 0^+) = \frac{\bar{\Delta}_2^2 \bar{\Delta}_4^2}{\bar{\Delta}_1^2 \bar{\Delta}_3^2 \bar{\Delta}_5^2 \bar{G}_6''} = \sqrt{\frac{3\pi}{2}} \frac{1}{\Delta_3}. \quad (14)$$

Hence,

$$\bar{G}_6'' = \frac{8}{5} \sqrt{\frac{2}{3\pi}} \frac{1}{\Delta_3}. \quad (15)$$

Thus we obtain,

$$\sigma_{xx}^{\text{dc}} \simeq \frac{\chi_{\text{csr}}(n)}{\Delta_1^2(n)} \times \sqrt{\frac{3\pi}{2}} \times \frac{5\Delta_2^2 \Delta_4^2}{8\Delta_5^2 \Delta_3}. \quad (16)$$

Physically, χ_{csr} measures the HCB kinetic energy and Δ_1^2/Δ_2 describes the current dissipation rate. The factors of $n(1-n)$ factors cancel out between χ_{csr} and Δ_1^2 . This can explain the approximate density independence of the conductivity found by Gaussian extrapolation in Section III A and shown in Fig. 1.

We ignore the weak density dependence of the leading order in β we invert σ_{xx}^{dc} to obtain the high temperature resistivity,

$$R_{xx} \simeq 3.3 \frac{h}{q^2} \frac{T}{t}. \quad (17)$$

Here we have not calculated the next order β^3 correction of σ_{xx}^{dc} as a function of density. We note that Ref. [19] found for $n = 0.5$ a relative correction $-0.75 \left(\frac{t}{T}\right)^2$, which at $T = 4T_{\text{BKT}}$ is less than 10%.

IV. HALL COEFFICIENT

The Hall coefficient formula [22] contains two contributions,

$$R_{\text{H}} = R_{\text{H}}^{(0)} + R_{\text{H}}^{\text{corr}}. \quad (18)$$

The first term is given by

$$R_{\text{H}}^{(0)} = \frac{\chi_{\text{cmc}}}{\chi_{\text{csr}}^2}. \quad (19)$$

The current-magnetization-current (CMC) susceptibility expanded to order $(\beta t)^2$ is

$$\begin{aligned} \chi_{\text{cmc}} &= 2(j^y, [M, j^x]) \\ &= 4 \frac{\beta^2 q^3 t^4}{c} (1-2n)n(1-n) \left(1 - (\beta t)^2 (1-3n(1-n)) \right). \end{aligned} \quad (20)$$

Note that χ_{csr} (χ_{cmc}) is ‘‘particle-hole’’ symmetric (anti-symmetric) under $n \rightarrow 1-n$. Thus we obtain,

$$R_{\text{H}}^{(0)} = \frac{1}{qc} \left(\frac{2n-1}{n(n-1)} + \frac{2}{3} (\beta t)^2 \left(n - \frac{1}{2} \right) \right). \quad (21)$$

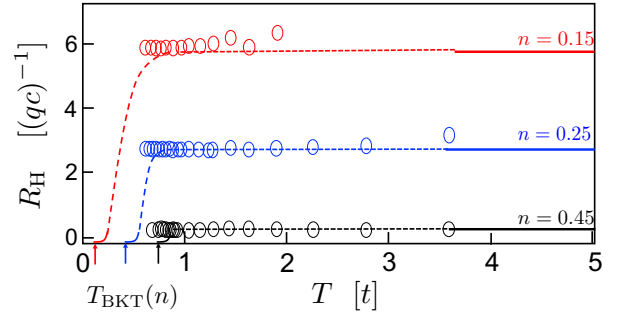


FIG. 5. Metallic Hall resistivity of HCB. High temperature asymptotes $R_{\text{H}}^{(0)}$ of Eq. (21) (solid lines), and lower temperature extension by QMC calculations (circles). Dashed lines interpolate between $R_{\text{H}}^{(0)}(T)$ and HN theory near $T_{\text{BKT}}(n)$, see Section V

We note that at low density, the Hall coefficient recovers the continuum Galilean invariant result $R_{\text{H}}^{(0)} \rightarrow (nqc)^{-1}$. Near half-filling, $R_{\text{H}} \sim -8(n - \frac{1}{2})/(qc)$ reflecting the effects of lattice Umklapp and hard core scattering.

Eq. (21) was extended to lower temperatures numerically by a path-integral based QMC for bosonic lattice models [28] which are devoid of a sign problem. We studied 24×24 size lattices, which was sufficiently large for expectation values at temperatures higher than T_{BKT} . The number of Monte Carlo sweeps was $\sim 5 \times 10^6$. β was subdivided into intervals $\epsilon = \beta/N_\epsilon$, $N_\epsilon = 10$. Off-diagonal operators (e.g. $S_i^+ S_j^-$, $S_i^+ S_j^z S_k^-$) were calculated using worm-type updates. In Fig. 5, the solid lines are the analytical results of Eq. (21), while the QMC data are depicted by open circles. We see that the Hall coefficients above the HN regime, rapidly saturate to their high temperature limit.

A. The Correction term

The correction term in Eq. (18) contains a sum of susceptibilities of Krylov operators:

$$\begin{aligned} R_{\text{H}}^{\text{corr}} &= \frac{1}{\chi_{\text{csr}}} \sum_{i,j=0}^{\infty} R_i R_j (1 - \delta_{i,0} \delta_{j,0}) M_{2i,2j}'' \\ M_{2i,2j} &= \text{Im} (\langle 2i; y | \mathcal{M} | 2j; x \rangle - \langle 2i; x | \mathcal{M} | 2j; y \rangle), \\ R_{i>1} &= \prod_{r=1}^i \left(-\frac{\Delta_{2r-1}}{\Delta_{2r}} \right), \quad R_0 = 1. \end{aligned} \quad (22)$$

The conductivity recurrences Δ_n are evaluated in Fig. 3. The unnormalized matrix elements M_{nm}'' of Eq. (22) involve susceptibilities of the form

$$\tilde{M}_{nm}'' = (\mathcal{L}^n j^y, [M, \mathcal{L}^m j^x]). \quad (23)$$

Unnormalized hyperstates can be expanded in terms of

the orthonormal Krylov bases by the Gram-Schmidt matrix K ,

$$\mathcal{L}^n j^\alpha = \sum_{k'=0}^k K_{n,k'} |k', \alpha\rangle, \quad (24)$$

where $\langle k, \alpha | k', \alpha' \rangle = \delta_{kk'} \delta_{\alpha\alpha'}$. The factors R_i involve a finite number of recurrences $\Delta_1, \dots, \Delta_{2i}$, which also determine K^{-1} up to the same order.

The simplicity of the Hamiltonian permits a calculation of up to fourth order corrections,

$$R_i R_j M''_{2i,2j}, \quad i, j = 0, 2, 4. \quad (25)$$

The magnetization matrix elements involved traces over up to $\sim 10^7$ operator products. The hypermagnetization matrix elements M''_{nm} , which are listed in Table II of Appendix C.

Since the Hall coefficient is finite for a metal, the summation over all the higher order corrections must converge. The corrections to $R_H^{(0)}$ up to fourth order are depicted in Fig. 2. We see that these corrections do not qualitatively change the zeroth term's behavior especially near the densities $n = 0, 1, \frac{1}{2}$, although they converge slower around intermediate densities $n = 0.25, 0.75$.

In conclusion, $R_H^{(0)}$ appears to be a qualitatively correct approximation at high temperatures. $T > t$.

In the lower temperature regime $R_H^{(0)}$, as evaluated by QMC, appears to be blind to the onset of long range phase correlations and vortex fluctuations as described by HN theory. This implies imply that that the correction term should grow in magnitude as $T \rightarrow T_{\text{BKT}}$, and approach $R_H^{\text{corr}} \rightarrow -R_H^{(0)}$, to comply with the onset of superconductivity.

V. MATCHING HALPERIN-NELSON THEORY

Halperin and Nelson (HN) described a narrow fluctuation region just above the two dimensional superconducting transition at T_{BKT} . In that regime, the resistivity tensor is dominated by the exponentially small density of free vortices which vanishes T_{BKT} . At higher temperatures, the vortex density increases such that they cease to be well defined degrees of freedom. According to (HN) theory [13],

$$\begin{aligned} R_{\alpha\beta}^{\text{HN}} &\simeq 2.7 R_{\alpha\beta}^{\text{n}}(T) \left(\frac{\xi_{\pm}}{\xi_c} \right)^{-2} \\ &= 2.7 R_{\alpha\beta}^{\text{n}}(T) \exp \left(-2b \left(\frac{T_{\text{BKT}}}{T - T_{\text{BKT}}} \right)^{\frac{1}{2}} \right). \end{aligned} \quad (26)$$

ξ_{\pm} is the BKT correlation length, and ξ_c is of the order of the HCB lattice constant and $b \simeq 1$.

For the HCB model, the “normal state” resistivities $R_{xx}^{\text{n}}(T)$ and $R_{yx}^{\text{n}}(T)$, is taken from our Eq. (17) (21), respectively.

We use these values to plot the crossovers from HN theory Eq. (26) to higher temperatures as dashed lines in Figs. 1 and 5.

VI. THERMAL HALL COEFFICIENT

The heat currents are defined using the energy polarization \mathbf{P}_E , and charge current \mathbf{j} ,

$$\begin{aligned} \mathbf{j}_Q &= i[H, \mathbf{P}_E] - \frac{\mu}{q} \mathbf{j} \\ \mathbf{P}_E &= \sum_{\langle ij \rangle} \frac{\mathbf{x}_i + \mathbf{x}_j}{2} h_{ij}, \\ h_{ij} &= -t (S_i^+ S_j^- + S_i^- S_j^+). \end{aligned} \quad (27)$$

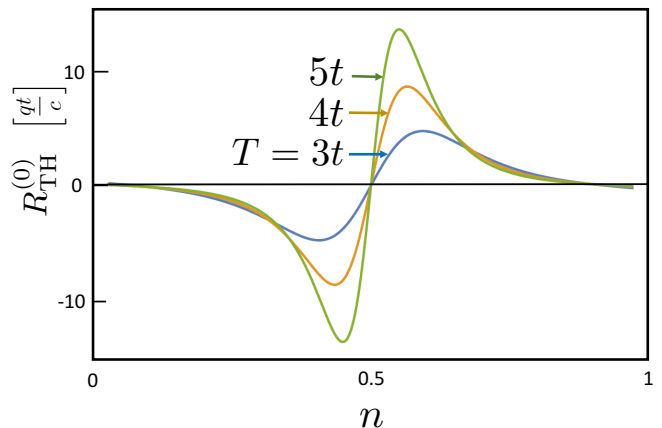


FIG. 6. Thermal Hall coefficient of HCB versus density at three high temperatures.

The zeroth thermal Hall coefficient is given by [22],

$$R_{\text{TH}}^{(0)} = \frac{\chi_{\text{cmc}}^{\text{Q}}}{\beta(\chi_{\text{csr}}^{\text{Q}})^2}, \quad (28)$$

where the heat current susceptibilities [29] are decomposed into energy-energy (EE) currents, energy-charge (EC) and the previously introduced charge-charge susceptibilities $\chi_{\text{cmc}}, \chi_{\text{csr}}$:

$$\begin{aligned} \chi_{\text{csr}}^{\text{Q}} &= (j_Q^x | j_Q^x) = \chi_{\text{csr}}^{\text{ee}} - \frac{2\mu}{q} \chi_{\text{csr}}^{\text{ec}} + \left(\frac{\mu}{q} \right)^2 \chi_{\text{csr}}, \\ \chi_{\text{cmc}}^{\text{Q}} &= 2(j_Q^y | M | j_Q^x) = \chi_{\text{cmc}}^{\text{ee}} - \frac{2\mu}{q} \chi_{\text{cmc}}^{\text{ec}} + \left(\frac{\mu}{q} \right)^2 \chi_{\text{cmc}}. \end{aligned} \quad (29)$$

The energy-energy susceptibilities are

$$\begin{aligned}\chi_{\text{csr}}^{\text{ee}} &= \beta t^4 n(6 - 14n + 16n^2 - 8n^3), \\ \chi_{\text{cmc}}^{\text{ee}} &= \frac{q\beta^2 t^6}{c} (24n - 112n^2 + 208n^3 - 200n^4 + 80n^5).\end{aligned}\quad (30)$$

The energy-charge susceptibilities are

$$\begin{aligned}\chi_{\text{csr}}^{\text{ec}} &= \frac{3q\beta^2 t^4}{2} (2n - 1)(1 - (2n - 1)^2), \\ \chi_{\text{cmc}}^{\text{ec}} &= -\frac{q^2 \beta t^4}{2} (1 - (2n - 1)^4).\end{aligned}\quad (31)$$

At high temperatures, the chemical potential μ is given by

$$e^{\beta\mu} = \frac{n}{1-n} \Rightarrow \mu(\beta) = \beta^{-1} \log\left(\frac{n}{1-n}\right). \quad (32)$$

In Fig. 6 we plot the zeroth thermal Hall coefficient defined in Eq. (28) for three high temperatures. $R_{\text{TH}}^{\text{corr}}$, and higher order in β corrections are not included here.

Since $\mu \sim 4\beta^{-1}(n - \frac{1}{2})$, by Eq. (31), the leading contribution at high temperature near half filling is coming from the contribution of

$$-2\frac{\mu}{q}\chi_{\text{cmc}}^{\text{ec}} \propto -\left(n - \frac{1}{2}\right). \quad (33)$$

The other $\mathcal{O}(\beta^0)$ term goes as $\mu^2\chi_{\text{cmc}} \sim (n - \frac{1}{2})^3$, which is subdominant near half filling. Therefore R_{TH} near half filling ends up having the opposite sign to the charge Hall coefficient. This (a-priori unexpected) result can be viewed as a “cooling” effect of the charge Hall current on the transverse temperature difference.

VII. DISCUSSION AND SUMMARY

The resistivity, Hall and thermal Hall coefficients were calculated for the metallic phase of HCB at temperatures above the HN superconducting fluctuations regime.

Near half filling, HCB cannot be reasonably approximated by weakly interacting quasiparticles. The model includes quantum mechanical effects of lattice periodicity combined with strong local constraints of no-double occupancies. The resulting conductivities can be classified as “non-Fermi liquid” metallic transport. The strong interactions strongly affect the moments of conductivity and the resulting magnitude of the linearly increasing resistivity.

The sign reversal of the Hall coefficient at half filling is also understood as an effect of strong repulsive interactions. HCB differ from continuum bosons, which are not expected to reverse their Hall sign as a function of filling [30].

Incidentally, we note that HCB and the tJ model of electrons [31] are somewhat similar in their proximity to Mott insulators. The Hall sign the tJ model also diverges toward the Mott phase, and exhibits a sign reversal relative to weakly interacting quasiparticles.

Experiments – HCB may be realized in low capacitance gated Josephson arrays at incommensurate fillings [32]. Measurements of temperature and density dependent resistivity and Hall coefficient could be compared to Figs. 1, 5, and 6 respectively.

The phase diagram of layered superconducting cuprates has been described by the classical (highly anisotropic) layered XY model [7, 33]. This description is supported by Uemura’s empirical relations between superfluid stiffness and T_c [34, 35]. It is therefore natural to study Eq. (1) in order to understand dynamical responses slightly above T_c .

Systematic studies [36, 37] have found an empirical proportionality between the resistivity slopes of *optimally doped* cuprates, and the inverse zero temperature superconducting stiffness. It is quite natural for HCB which are governed by the single energy scale t governing both quantities. The linearly rising resistivity in Fig. 1 suggests that one should consider that a significant part of the transport current, slightly above T_c , may be effectively carried by HCB that describe preformed (tightly bound) Cooper pairs. This may resolve some of the “bad metal” conundrum [38] in which the large magnitude of resistivity seems inconsistent with well defined Fermi liquid quasiparticles.

Finally, cold bosonic atoms trapped on optical lattices can serve as platforms for measuring HCB conductivities using time dependent potentials. A Hall effect can be induced by artificial gauge fields [39–41]. We hope our results will motivate such experiments.

Acknowledgements – We thank Anna Keselman and Abhisek Samanta for consultations in the numerical implementation. The QMC calculations were done with the help of the DSQSS package and S.B. sincerely thanks Naoki Kawashima and Yuichi Motoyama for their kind help. AA acknowledges the Israel Science Foundation (ISF) Grant No. 2081/20. S.G. acknowledges support from the Israel Science Foundation (ISF) Grant no. 586/22 and the US–Israel Binational Science Foundation (BSF) Grant no. 2020264. This work was performed in part at the Aspen Center for Physics, which is supported by National Science Foundation grant PHY-2210452, and at the Kavli Institute for Theoretical Physics, supported by Grant Nos. NSF PHY-1748958, NSF PHY-1748958 and NSF PHY-2309135.

Appendix A: Calculating recurrences from moments

The moments are related to the recurrences by the matrix equation [19],

$$\mu_{2k} = \chi_{\text{csr}}(L^{2k})_{00}, \quad (\text{A1})$$

where the tridiagonal Liouvillian matrix is defined as,

$$L_{ij}[\Delta] = \begin{pmatrix} 0 & \Delta_1 & 0 & 0 & 0 & \dots \\ \Delta_1 & 0 & \Delta_2 & 0 & 0 & \dots \\ 0 & \Delta_2 & 0 & \Delta_3 & 0 & \dots \\ 0 & 0 & \Delta_3 & 0 & \Delta_4 & \dots \\ 0 & 0 & 0 & \Delta_4 & 0 & \dots \\ 0 & \vdots & \vdots & \vdots & \vdots & \dots \end{pmatrix} \quad (\text{A2})$$

Taking even powers of L and evaluating their (00) matrix elements, yields relations between μ_{2k} and the preceding recurrences $\Delta_1, \dots, \Delta_k$, which are symbolically solved to obtain Eqs. (8).

Appendix B: High temperature expansions of susceptibilities

We use the XY model representation, Eq. (1) to derive the following high temperature results. In the grand canonical ensemble, the mean magnetization for the XY model $m = 2n - 1$, where $0 \leq n \leq 1$ is the HCB density per site, can be imposed at infinite temperature by a product density matrix $\rho_0(\delta)$, with a fugacity parameter δ :

$$\rho_0(\delta) = \prod_i \left(\frac{1+\delta}{2} |\uparrow\rangle\langle\uparrow| + \frac{1-\delta}{2} |\downarrow\rangle\langle\downarrow| \right), \quad (\text{B1})$$

where the average magnetization at infinite temperature is

$$m(0) = \langle 2S_i^z \rangle_{\beta=0} \equiv \delta. \quad (\text{B2})$$

Expectation values are,

$$\begin{aligned} \text{Tr} \rho_0 S_i^x &= 0, \\ \text{Tr} \rho_0 S_i^y &= 0, \\ \text{Tr} \rho_0 S_i^z &= \frac{1}{2} \delta. \end{aligned} \quad (\text{B3})$$

At finite temperature, we expand the average magnetization $m(\delta)$ to second order in β ,

$$\begin{aligned} m &= \frac{\text{Tr} \rho_0(\delta) e^{-\beta H} 2S_i^z}{\text{Tr} \rho_0(\delta_0) e^{-\beta H}} = \delta + \frac{\beta^2}{2} \text{Tr} \rho_0(\delta) H^2 (2S_i^z - \delta) \\ &= \delta - \beta^2 \delta (1 - \delta^2) + \mathcal{O}(\beta^4). \end{aligned} \quad (\text{B4})$$

Eq. (B4) allows us to evaluate the magnetization dependence of a δ -dependent susceptibility by

$$\chi(\delta, \beta) = \chi(m + \beta^2 \delta (1 - \delta^2), \beta). \quad (\text{B5})$$

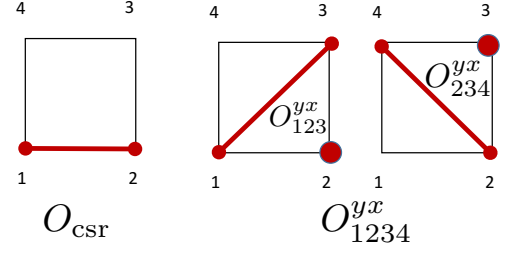


FIG. 7. Operators which are averaged over in the CSR and CMC. Line denotes a bond operator ($S_i^+ S_j^- + (i \leftrightarrow j)$) and the circle denotes a site operator S_i^z , respectively.

The coefficients in the high temperature expansion of the susceptibilities are found using a numerical symbolic multiplication method, described in Appendix D. Here, we outline the scheme by two simplest examples- the CSR and CMC, defined in Eq. (7) and Eq. (20) respectively.

1. CSR

The CSR is given by averaging the single bond operator, shown in Fig. 7. The first two leading orders in (βt) of the CSR are defined as,

$$\bar{\chi}_{\text{csr}} = q^2 \beta t^2 \bar{\chi}_{\text{csr}}^{(1)} + q^2 \beta^3 t^4 \bar{\chi}_{\text{csr}}^{(3)} + \dots \quad (\text{B6})$$

where,

$$\bar{\chi}_{\text{csr}}^{(1)} = \frac{1}{2} (1 - m^2). \quad (\text{B7})$$

The graphs contributing to the order β^3 CSR are shown in Fig. 8. The result (using symbolic multiplication) is-

$$\bar{\chi}_{\text{csr}}^{(3)}(\delta) = \frac{\beta^3}{24} (-1 + 20\delta^2 - 19\delta^4). \quad (\text{B8})$$

Upon transforming this using Eq. (B5), one gets-

$$\begin{aligned} \chi_{\text{csr}}^{(3)}(m) &= \lim_{\delta \rightarrow m} \{ \chi_{\text{csr}}^{(3)}(\delta) - (\partial_\delta \chi_{\text{csr}}^{(1)}) \delta (1 - \delta^2) \} \\ &= \frac{1}{24} (-1 - 4m^2 + 5m^4). \end{aligned} \quad (\text{B9})$$

Finally, if one substitutes $m = 2(n - \frac{1}{2})$ in Eq. B7 and Eq. B8 in Eq. B6, we obtain Eq. (7).

2. CMC

The CMC is given by averaging the plaquette operator, shown in Fig. 7.

$$\begin{aligned} \chi_{\text{cmc}} &= -2q^3 t^2 \langle O_{123}^{yx} \rangle \\ &= 2q^3 t^2 \langle (S_1^+ S_3^- + S_1^- S_3^+) S_2^z \rangle, \end{aligned} \quad (\text{B10})$$

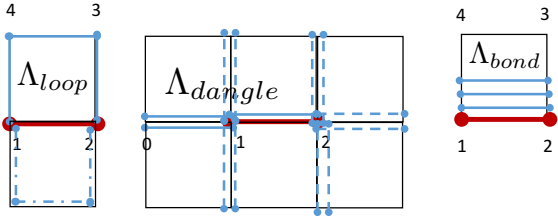


FIG. 8. Graphs of operators which contribute to CSR at $\mathcal{O}(\beta^3)$.

where we have used using C4 symmetry to equate four identical contributions to the expectation value. The leading order $\chi_{\text{cmc}}^{(2)}$ requires tracing O_{123}^{yx} times two Hamiltonian bonds in a connected cluster inside a plaquette. The calculation yields

$$\begin{aligned}\chi_{\text{cmc}}^{(2)} &= -\text{Tr}\rho_0(\beta H)^2 O_{123}^{yx} \\ &= -\frac{(\beta t)^2}{2} m(1-m^2).\end{aligned}\quad (\text{B11})$$

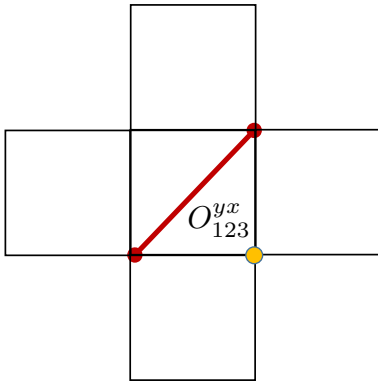


FIG. 9. Minimal connected cluster for the calculation of $\chi_{\text{cmc}}^{(4)}$, which must include 4 powers of H whose bonds connect to the sites of O_{123}^{yx} and contribute to a non vanishing trace.

The order β^4 contribution to CMC is obtained to be-

$$\chi_{\text{cmc}}^{(4)}(\delta) = \frac{(\beta t)^4}{24} (15\delta - 42\delta^3 + 27\delta^5).\quad (\text{B12})$$

The minimal cluster chosen for this computation is shown in Fig. 9. Transforming the expression using Eq. (B5), yields

$$\begin{aligned}\chi_{\text{cmc}}^{(4)}(m) &= \lim_{\delta \rightarrow m} \{\chi_{\text{cmc}}^{(4)}(\delta) - (\partial_\delta \chi_{\text{cmc}}^{(4)})\delta(1-\delta^2)\} \\ &= \frac{(\beta t)^4 m}{8} (1-m^2)(1+3m^2).\end{aligned}\quad (\text{B13})$$

Again, combining Eq. B11 and Eq. B12, replacing $m = 2(n - \frac{1}{2})$ in Eq. B10 we obtain Eq. (20).

3. Thermal susceptibilities

The thermal currents are defined in Eq. (27). In the CMC susceptibilities used in Eq. (29) we use the electric magnetization M as defined in Eq. (2). The chemical potential μ at high temperatures is related to the density by solving the single-site problem (neglecting the βH term), which yields Eq. (32),

$$n = \frac{e^{\beta\mu}}{1 + e^{\beta\mu}} \Rightarrow \mu(\beta) = \beta^{-1} \log\left(\frac{n}{1-n}\right).\quad (\text{B14})$$

The new susceptibilities required to determine the thermal Hall coefficient ($\chi_{\text{csr}}^{\text{ee}}, \chi_{\text{cmc}}^{\text{ee}}, \chi_{\text{csr}}^{\text{ec}}$ and $\chi_{\text{cmc}}^{\text{ec}}$) were all evaluated using the methods explained in Appendix D. The energy current itself turns out to be a combination of three-site operators, containing next-nearest neighbour currents decorated with S^z operators at nearest-neighbour locations. Hence, the resulting susceptibilities turn out to be more complicated and have different β dependencies to leading order compared to the charge case. One finds the following expressions-

$$\begin{aligned}\chi_{\text{csr}}^{\text{ee}} &= \beta t^4 \left(1 - \frac{m^2}{2} - \frac{m^4}{2}\right), \\ \chi_{\text{cmc}}^{\text{ee}} &= \frac{q\beta^2 t^6}{c} \left(\frac{-7m}{2} + m^3 + \frac{5m^5}{2}\right), \\ \chi_{\text{csr}}^{\text{ec}} &= \frac{3q\beta t^4}{2} m(1-m^2), \\ \chi_{\text{cmc}}^{\text{ec}} &= -\frac{q^2 \beta t^4}{2} (1-m^4).\end{aligned}\quad (\text{B15})$$

Now, at low β (high temperatures), Eq. (29) shows that χ_{csr}^Q is dominated by $(\frac{\mu}{q})^2 \chi_{\text{csr}}$ (the charge CSR term), which is $\mathcal{O}(1/\beta)$ and both $-2(\frac{\mu}{q}) \chi_{\text{cmc}}^{\text{ec}}$ and $(\frac{\mu}{q})^2 \chi_{\text{cmc}}^{\text{ec}}$ contributions are important ($\mathcal{O}(1)$) in χ_{cmc}^Q .

However, one also observes that the susceptibilities (as well as μ) have different density dependencies near half-filling. For instance, μ , $\chi_{\text{csr}}^{\text{ec}}$, $\chi_{\text{cmc}}^{\text{ee}}$ and $\chi_{\text{cmc}}^{\text{ec}}$ cross zero at $n = \frac{1}{2}$ by particle-hole symmetry / anti-symmetry, while the thermoelectric CMC ($\chi_{\text{cmc}}^{\text{ec}}$) is a very flat function of n near half-filling. Hence, the sign of the thermal Hall coefficient is determined by $\chi_{\text{ec}}^{\text{cmc}}$ and turns out to be opposite to the charge case near $n = \frac{1}{2}$.

Appendix C: Computing the correction term

The normalized matrix elements of Eq. (22) require expanding the operators $\mathcal{L}^{2k} j^\alpha$ in the Krylov basis

a	b	$\chi_{\text{csr}} \tilde{M}_{ab} / (\beta^2 q^3 t^{(a+b+4)})$
0	0	$-m(1-m^2)$
0	2	$-\frac{1}{2}m(1-m^2)^2$
0	4	$-\frac{1}{2}(56m + 181m^3 - 194m^5 + 69m^7)$
2	0	$-m(1-m^2)^2$
2	2	$\frac{1}{2}(36m - 53m^3 - 2m^5 + 19m^7)$
2	4	$\frac{1}{2}(1871m - 2638m^3 - 1017m^5 + 2464m^7 - 680m^9)$
4	0	$m(1-m^2)^3$
4	2	$\frac{1}{2}(1307m - 2476m^3 + 969m^5 + 262m^7 - 62m^9)$
4	4	$\frac{1}{2}(115281m - 240247m^3 + 109284m^5 + 39594m^7 - 22457m^9 - 1455m^{11})$

TABLE II. Charge hypermagnetization matrix elements (unnormalized) at $T = \infty$.

$|k; \alpha\rangle$ [22]. Using

$$\mathcal{L}^k j^\alpha = \sum_{k'} |k'; \alpha\rangle \langle k'; \alpha| \mathcal{L}^k |0; \alpha\rangle = \chi_{\text{csr}} \sum_{k'} K_{k,k'} |k'; \alpha\rangle \quad (\text{C1})$$

where $K_{k',k} = (L^k)_{k',0}$ are functions of a finite number of recurrences, $\Delta_1, \dots, \Delta_{k' \leq k}$. Using

$$|k, \alpha\rangle = K_{k,k'}^{-1} \mathcal{L}^{k'} |0\rangle \quad (\text{C2})$$

we can transform any normalized matrix element of the hypermagnetization into unnormalized matrix elements

$$\tilde{M}_{n'm'} = \langle 0, y | \mathcal{L}^{n'} \mathcal{M} \mathcal{L}^{m'} | 0, x \rangle, \quad (\text{C3})$$

which are easier to calculate, using

$$M''_{n,m} = \sum_{n' \leq n} \sum_{m' \leq m} K_{n,n'}^{-1} K_{m,m'}^{-1} \tilde{M}''_{n',m'}. \quad (\text{C4})$$

The latter are computed using the methods described in Appendix D are quoted in Table II.

Appendix D: Automated evaluation of operator traces

High order moments $\mu_{2k}, k = 0 \dots 5$, recurrences $\Delta_{k < 5}$ and hypermagnetization matrix elements $\tilde{M}_{nm}, nm \leq 4$ require traces over a large number of site-operators products on square lattice. We've used symbolic multiplication to perform these traces.

The clusters are formed by commuting bond operators of the Hamiltonian or magnetization with the root current operator $j_{\langle ij \rangle}^\alpha$ on a single bond $\langle ij \rangle$ (utilizing translational symmetry). The result of $\mathcal{L}^n j_i^\alpha$ is a sum of multi-site products of operators $O_{i_1}(\mathbf{r}_1) \cdot O_{i_2}(\mathbf{r}_2) \cdot \dots \cdot O_{i_N}(\mathbf{r}_N)$, which is treated as a new ‘‘hyperstate’’ with a complex amplitude that is stored separately.

The rapid (factorial) growth of the number of such operator products limited extending our calculations beyond

$n = 4$. At fourth order we calculated traces over $\sim 10^7$ operators.

The new hyperstates are generated using the site-local operator multiplication table,

$$\sigma_i \sigma_j = \delta_{ij} + i \epsilon_{ijk} \sigma_k, \quad (\text{D1})$$

where σ_i 's are usual Pauli spin matrices. We performed the calculations on a 24×24 square grid, which ensured that the even the largest operator products were contained within the lattice. After constructing the operators, we multiplied them with powers of the Hamiltonian (also a collection of bond operators) to ensure that they had a non-vanishing trace. Most of the resulting hyperstates have zero trace, owing to unmatched Pauli matrices

$$\text{Tr}(\sigma_i^x) = \text{Tr}(\sigma_i^y) = 0. \quad (\text{D2})$$

The computation was reduced by eliminating operators with unmatched σ^x 's or σ^y 's. Moreover, we combined equal operator products at intermediate stages, to retain only distinct hyperstates. This sorting becomes time consuming at about 10^6 operators. Finally, we evaluated the traces over the remaining density (σ^z) factors,

$$\text{Tr}(\sigma_i^z) = \delta = m|_{\beta=0}, \quad (\text{D3})$$

as given in Appendix B.

Appendix E: QMC calculation of the Hall coefficient

In this short section, we provide a few details of the QMC calculation, used to generate the lower temperature results for $R_H^{(0)}$, as depicted in Fig. 5. We've used the DSQSS package [28] for this purpose. This package employs a path-integral based Monte Carlo scheme for bosons and quantum spin systems, devoid of a sign problem. More specifically, it uses the Directed Loop Algorithm (DLA) [42]. In DLA, one adds a pair of ‘worm heads’ at two randomly chosen space-time points within the simulation. These represent insertions of off-diagonal operators (like S^x). Thereafter, one of these is kept fixed (called the ‘tail’), while the other ‘propagates’ obeying detailed balance rules. In course of propagation, the head scatters off ‘vertices’, which are two-spin operators specific to the Hamiltonian in question. Finally, one terminates the propagation when the head meets the tail. The ‘closed loop’ configurations thus obtained contribute to the free energy. The statistics obtained from the worm propagation moves (while the loop is open) corresponding to a fixed space-time separation of the worm head and tail directly provide an estimate for the two-point off-diagonal correlation functions (like $\langle S_i^+(\tau) S_j^-(0) \rangle$). We used the equal-time ($\tau = 0$) results for our purpose. For the operators shown in Fig. 7, one can directly use this result (for nearest-neighbour separation) to calculate

the CSR, while for the CMC, one has to ‘re-weight’ the measurements (for next-nearest neighbour separation) by

the S^z value of the spin at the nearest neighbour location. We achieved this by slightly modifying the correlation function measurement part of the source code.

-
- [1] Takeo Matsubara and Hirotugu Matsuda. A lattice model of liquid helium, i. *Progress of Theoretical Physics*, 16(6):569–582, 1956.
- [2] Ehud Altman and Assa Auerbach. Oscillating superfluidity of bosons in optical lattices. *Physical review letters*, 89(25):250404, 2002.
- [3] Christian Gross and Immanuel Bloch. Quantum simulations with ultracold atoms in optical lattices. *Science*, 357(6355):995–1001, 2017.
- [4] A Kremen, H Khan, YL Loh, TI Baturina, N Trivedi, A Frydman, and B Kalisky. Imaging quantum fluctuations near criticality. *Nature physics*, 14(12):1205–1210, 2018.
- [5] Ehud Altman and Assa Auerbach. Haldane gap and fractional oscillations in gated josephson arrays. *Physical review letters*, 81(20):4484, 1998.
- [6] Ehud Altman and Assa Auerbach. Plaquette boson-fermion model of cuprates. *Physical Review B*, 65(10):104508, 2002.
- [7] Alexander Mihlin and Assa Auerbach. Temperature dependence of the order parameter of cuprate superconductors. *Physical Review B*, 80(13):134521, 2009.
- [8] E Loh Jr, DJ Scalapino, and PM Grant. Monte carlo studies of the quantum xy model in two dimensions. *Physical Review B*, 31(7):4712, 1985.
- [9] H-Q Ding and MS Makivic. Kosterlitz-thouless transition in the two-dimensional quantum xy model. *Physical Review B*, 42(10):6827, 1990.
- [10] G. G. Batrouni and R. T. Scalettar. Phase separation in supersolids. *Phys. Rev. Lett.*, 84:1599–1602, Feb 2000.
- [11] VL314399 Berezinskii. Destruction of long-range order in one-dimensional and two-dimensional systems having a continuous symmetry group i. classical systems. *Sov. Phys. JETP*, 32(3):493–500, 1971.
- [12] John Michael Kosterlitz and David James Thouless. Ordering, metastability and phase transitions in two-dimensional systems. *Journal of Physics C: Solid State Physics*, 6(7):1181, 1973.
- [13] BI Halperin and David R Nelson. Resistive transition in superconducting films. *Journal of low temperature physics*, 36:599–616, 1979.
- [14] Snir Gazit, Daniel Podolsky, Assa Auerbach, and Daniel P. Arovas. Dynamics and conductivity near quantum criticality. *Phys. Rev. B*, 88:235108, Dec 2013.
- [15] Samuel Lederer, Yoni Schattner, Erez Berg, and Steven A. Kivelson. Superconductivity and non-fermi liquid behavior near a nematic quantum critical point. *Proceedings of the National Academy of Sciences*, 114(19):4905–4910, 2017.
- [16] Hazime Mori. Transport, collective motion, and brownian motion. *Progress of theoretical physics*, 33(3):423–455, 1965.
- [17] Robert Zwanzig. *Nonequilibrium statistical mechanics*. Oxford university press, 2001.
- [18] VS Viswanath and Gerhard Müller. *The recursion method: application to many body dynamics*, volume 23. Springer Science & Business Media, 1994.
- [19] Netanel H Lindner and Assa Auerbach. Conductivity of hard core bosons: A paradigm of a bad metal. *Physical Review B*, 81(5):054512, 2010.
- [20] Ilia Khait, Snir Gazit, Norman Y Yao, and Assa Auerbach. Spin transport of weakly disordered Heisenberg chain at infinite temperature. *Physical Review B*, 93(22):224205, 2016.
- [21] Assa Auerbach. Hall number of strongly correlated metals. *Physical Review Letters*, 121(6):066601, 2018.
- [22] Assa Auerbach. Equilibrium formulae for transverse magnetotransport of strongly correlated metals. *Physical Review B*, 99(11):115115, 2019.
- [23] Abhisek Samanta, Daniel P Arovas, and Assa Auerbach. Hall coefficient of semimetals. *Physical Review Letters*, 126(7):076603, 2021.
- [24] Wen O. Wang, Jixun K. Ding, Brian Moritz, Edwin W. Huang, and Thomas P. Devereaux. DC Hall coefficient of the strongly correlated Hubbard model. *npj Quantum Materials*, 5(1):51, 2020.
- [25] Ilia Khait, Sauri Bhattacharyya, Abhisek Samanta, and Assa Auerbach. Hall map and breakdown of fermi liquid theory in the vicinity of a mott insulator. *arXiv:2211.15711*, 2022.
- [26] H.-Q. Ding. Phase transition and thermodynamics of quantum xy model in two dimensions. *Phys. Rev. B*, 45:230–242, Jan 1992.
- [27] Kenji Harada and Naoki Kawashima. Universal jump in the helicity modulus of the two-dimensional quantum xy model. *Phys. Rev. B*, 55:R11949–R11952, May 1997.
- [28] Yuichi Motoyama, Kazuyoshi Yoshimi, Akiko Masaki-Kato, Takeo Kato, and Naoki Kawashima. Dsqqs: Discrete space quantum systems solver. *Computer Physics Communications*, 264:107944, 2021.
- [29] B Sriram Shastry. Sum rule for thermal conductivity and dynamical thermal transport coefficients in condensed matter. *Physical Review B*, 73(8):085117, 2006.
- [30] Sebastian D Huber and Netanel H Lindner. Topological transitions for lattice bosons in a magnetic field. *Proceedings of the National Academy of Sciences*, 108(50):19925–19930, 2011.
- [31] Ilia Khait, Sauri Bhattacharyya, Abhisek Samanta, and Assa Auerbach. Hall map and breakdown of fermi liquid theory in the vicinity of a mott insulator. *Arxiv:2211.15711*, 2022.
- [32] C. G. L. Bøttcher, F. Nichele, M. Kjaergaard, H. J. Suominen, J. Shabani, C. J. Palmstrøm, and C. M. Marcus. Superconducting, insulating and anomalous metallic regimes in a gated two-dimensional semiconductor–superconductor array. *Nature Physics*, 14(11):1138–1144, 2018.
- [33] Iulian Hetel, Thomas R Lemberger, and Mohit Randeria. Quantum critical behaviour in the superfluid density of strongly underdoped ultrathin copper oxide films. *Nat. Phys.*, 3(10):700–702, 2007.

- [34] YJ Uemura, GM Luke, BJ Sternlieb, JH Brewer, JF Carolan, W.N. Hardy, R Kadono, JR Kempton, RF Kiefl, SR Kreitzman, et al. Universal correlations between T_c and n/m^* (carrier density over effective mass) in high- T_c cuprate superconductors. *Physical review letters*, 62(19):2317, 1989.
- [35] I Božović, X He, J Wu, and AT Bollinger. Dependence of the critical temperature in overdoped copper oxides on superfluid density. *Nature*, 536(7616):309–311, 2016.
- [36] Shahaf Asban, Meni Shay, Muntaser Naamneh, Tal Kirzhner, and Amit Keren. Strong-versus weak-coupling paradigms for cuprate superconductivity. *Physical Review B*, 88(6):060502, 2013.
- [37] This behavior is also consistent with a combination of Uemura’s scaling of transition temperature with superfluid stiffness [34], the linear resistivity of clean optimally doped samples above T_c , and Homes law relation between superfluid stiffness and resistivity $R_{xx}(T_c)$ [43].
- [38] V. J. Emery and S. A. Kivelson. Superconductivity in bad metals. *Phys. Rev. Lett.*, 74:3253–3256, Apr 1995.
- [39] Lindsay J LeBlanc, Karina Jiménez-García, Ross A Williams, Matthew C Beeler, Abigail R Perry, William D Phillips, and Ian B Spielman. Observation of a superfluid hall effect. *Proceedings of the National Academy of Sciences*, 109(27):10811–10814, 2012.
- [40] Nathan Goldman, G Juzeliūnas, Patrik Öhberg, and Ian B Spielman. Light-induced gauge fields for ultracold atoms. *Reports on Progress in Physics*, 77(12):126401, 2014.
- [41] Jacob F Sherson, Christof Weitenberg, Manuel Endres, Marc Cheneau, Immanuel Bloch, and Stefan Kuhr. Single-atom-resolved fluorescence imaging of an atomic mott insulator. *Nature*, 467(7311):68–72, 2010.
- [42] Olav F. Syljuåsen and Anders W. Sandvik. Quantum monte carlo with directed loops. *Phys. Rev. E*, 66:046701, Oct 2002.
- [43] Christopher C Homes, SV Dordevic, T Valla, and M Strongin. Scaling of the superfluid density in high-temperature superconductors. *Physical Review B*, 72(13):134517, 2005.